Princeton Plasma Physics Laboratory

PPPL-5191

A Predictive Model for the Greenwald Density Limit

Q. Teng, D.P. Brennan, L. Delgado-Aparicio, D.A. Gates, J. Swerdlow and R.B. White

September 2015

Prepared for the U.S. Department of Energy under Contract DE-AC02-09CH11466.

Princeton Plasma Physics Laboratory
Report Disclaimers

Full Legal Disclaimer

Trademark Disclaimer

PPPL Report Availability

Princeton Plasma Physics Laboratory:

http://www.pppl.gov/techreports.cfm

Office of Scientific and Technical Information (OSTI):

http://www.osti.gov/scitech/

Related Links:

U.S. Department of Energy

U.S. Department of Energy Office of Science

U.S. Department of Energy Office of Fusion Energy Sciences

A Predictive Model for the Greenwald Density Limit

Q. Teng,[1] D.P. Brennan,[1] L. Delgado-Aparicio,[1] D.A. Gates,[1] J. Swerdlow,[1] and R.B. White[1]

[1]*Plasma Physics Laboratory, Princeton University,*

P.O. Box 451, Princeton, New Jersey 08543

(Dated: September 2, 2015)

Abstract

The Greenwald density limit is reproduced for the first time using a phenomenologically correct model with experiment-relevant parameters. A simple model of equilibrium and local power balance inside the island during its evolution has been implemented to calculate the radiation-driven thermo-resistive tearing mode growth and explain the density limit. Strong destabilization of the tearing mode due to an imbalance of local Ohmic heating and radiative cooling in the island predicts the density limit within a few percent with reasonable assumptions for impurity densities. Results are robust to a substantial variation in model parameters within the range of experiments.

The tokamak density limit is a ubiquitous phenomenon found in all tokamak experiments. The empirical scaling, known as the Greenwald density limit[1],

$$n_{\mathrm{G}} = \frac{I_{\mathrm{p}}}{\pi a^2} \tag{1}$$

is well established, where n_{G} is the line-averaged density in units of 10^{20} m^{-3}, the plasma current I_{p} is in MA and the minor radius a is in meters. Many attempts have been made to explain the mechanism behind the density limit. Earlier works have correctly related the density limit to the radiative collapse of the current profile and the emergence of magnetic islands, though no previous work has explained the limit quantitatively using reasonable parameters[2–4]. Recently D.A. Gates *et. al.* put forward a novel mechanism that explains the phenomenon using a thermo-resistive tearing mode formalism[5, 6]. R. B. White *et. al.* completed this model with a more profound understanding of tearing mode growth by taking the crucial island asymmetry term into account[7]. D. P. Brennan *et. al.* reproduced the exponential growth of the island, as predicted by the analytical cylindrical model, with a 3-D full MHD code DEBS[8]. Scanning the low- and high- Z impurity densities, L. Delgado-Aparicio found that the radiative power density can be significantly enhanced while still obtaining the experimental Z_{eff} values well within its error bars [6, 9]. As pointed out by Rebut *et. al.*[3], impurities in the magnetic island cool the island radiatively and counter the Ohmic heating. The power balance sets the internal temperature profile of the island. As plasma density is increased, the Ohmic heating typically decreases while the radiative cooling increases. When radiation losses dominate, the temperature drop creates a negative current perturbation inside the island. The current perturbation, coupled with the asymmetry of the island, can cause substantial growth of the island and lead to disruption. The island growth is very sensitive to radiative cooling and the cooling is sensitive to plasma density. We will show that local power balance inside the island is a very accurate criterion for the density limit.

In this work, we show that the thermo-resistive tearing mode model can explain the density limit quantitatively. The scan of plasma density is from 2×10^{19} m^{-3} to 2×10^{20} m^{-3}, with the deviation from the density limit being only 3%. The stiffness of this model is also shown by varying the parameters assumed in the model within the range of experiments. This work is focused on island growth at the $q = 2$ surface, but the model is applicable to the island on any rational surface. The magnetic island growth rate is calculated by the

modified Rutherford equation (MRE) [7]

$$\frac{dw}{dt} = \frac{1}{2}\left[\Delta'(w) + \Delta'_{\delta j}(w) + \Delta'_{A}(w)\right], \tag{2}$$

where t is normalized to $\tau_R = \mu_0 r_s^2/\eta$, r_s is the rational surface location normalized to minor radius, w is island width normalized to minor radius. $\Delta'(w)$ is the classical term first derived in [10]; $\Delta'_{\delta j}(w)$ is the contribution of the current perturbation; $\Delta'_{A}(w)$ is the contribution of the island asymmetry. For small island width, approximate expressions of $\Delta'_{\delta j}(w)$, $\Delta'_{A}(w)$ are derived [7],

$$\Delta'_{\delta j}(w) = 16\frac{\langle \delta j_1 \rangle}{\psi_0''}\frac{w}{w^2 + w_F^2},\ \Delta'_{A}(w) = \frac{2j'(r_x)}{\pi\psi_0''}\frac{w^2}{w^2 + w_F^2}Af_F, \tag{3}$$

where $\langle \delta j_1 \rangle$ is the current perturbation integrated over the island interior, ψ_0'' is the second derivative of zeroth order helical flux, w_F [11] is the Fitzpatrick critical island width accounting for small island effect, r_x is the location of x point, $A = (r_r - r_x)/(r_x - r_l) - 1$ is the island asymmetry, r_l and r_r are the left and right edges of the island at the maximum width, and f_F is the Fitzpatrick factor accounting for the degree of current profile flattening inside the island (f_F is chosen to be 1 in our calculation). As ψ_0'' and $j'(r_x)$ are always negative, $\Delta'_{\delta j}(w)$ (for a negative $\langle \delta j_1 \rangle$) and $\Delta'_{A}(w)$ are both destabilizing. The temperature profile inside the island is determined by,

$$\frac{\partial T}{\partial t} = \nabla \cdot (\chi_\perp \nabla T) + P_{\text{input}} - P_{\text{loss}}, \tag{4}$$

where $\chi_\perp$ is the cross field electron thermal diffusivity. As is shown in Ref. [7], in steady state, this second order differential equation can be simplified to a first order differential equation,

$$0 = \chi_\perp \psi_0''(r_s)\frac{dT}{d\psi} + P_{\text{input}} - P_{\text{loss}}, \tag{5}$$

where ψ is the helical flux. The boundary condition is set by the equilibrium temperature at the separatrix of the island. Thus net power loss (input) in the island would cause a drop (rise) in temperature. The temperature drop (rise) then causes a rise (drop) in resistivity and a negative (positive) current perturbation, destabilizing (stabilizing) the island growth. As has been shown in Ref. [7], a small amount of cooling power is enough to trigger a large island leading to disruption.

To associate the local power balance criterion with the global Greenwald density limit, a set of cylindrical tokamak-like equilibria is assumed. The current density profile is given

by[12]

$$j(r) = \frac{j_0}{\left[1 + (r/r_0)^{2\nu}\right]^{1+1/\nu}}, \tag{6}$$

and the safety factor profile is given by,

$$q(r) = q_0 \left[1 + (r/r_0)^{2\nu}\right]^{1/\nu}, \tag{7}$$

where j_0 is the current density on the axis, r_0 is the width of the current channel, ν is a parameter controlling the peakedness of the current profile, $q_0 = 2B_\phi/(\mu_0 R j_0)$ is the safety factor on the axis, B_ϕ is the toroidal magnetic field, R is the major radius. A parabolic density profile is also assumed

$$n_e = n_{e0}\left(1 - \left(\frac{r}{a}\right)^2\right), \tag{8}$$

where n_{e0} the plasma density on the axis, a is the minor radius. In this simplified cylindrical model, the equilibrium is set by three constraints. For each equilibrium, we choose a set of q_0, $q_{\rm edge}$ and plasma density n_e. The third parameter constraining the equilibrium ν is calculated with an *ad hoc* relation between plasma density and internal inductance. In cylindrical geometry, the internal inductance is defined as,

$$l_i = \frac{2\pi \int_0^a B_\phi^2(r) r dr}{\pi a^2 B_\phi^2(a)} \tag{9}$$

$$= 2\left[1 + \left(\frac{a}{r_0}\right)^{2\nu}\right]^{2/\nu} \int_0^a dr \frac{r^3}{a^4\left[1 + \left(\frac{r}{r_0}\right)^{2\nu}\right]^{2/\nu}}, \tag{10}$$

where $r_0 = \left[\left(\frac{q_{\rm edge}}{q_0}\right)^\nu - 1\right]^{-1/2\nu}$. In Figure 5 of Ref. [2], it is found experimentally (JET) that when approaching the density limit, the internal inductance increases. The upper limit of internal inductance at the density limit and the lower limit are fit by [5]

$$l_{i,max} = (0.12 q_{\rm edge} \cdot h + 0.6) \cdot h, \tag{11}$$

$$l_{i,min} = (-0.08 q_{\rm edge} \cdot h + 1.05) \cdot h, \tag{12}$$

where $q_{\rm edge} = 2\pi a^2 B_\phi(a)/(\mu_0 R I)$ is the safety factor at the edge, $h = (1+\kappa^2)/(2\kappa)$ approximates the modifications of internal inductance and safety factor due to elongation κ (here κ=1.9). In order to simulate the equilibrium evolution with increasing plasma density, we need the relation between internal inductance and plasma density which is not present

in published literature. To mimic experiments we assume an *ad hoc* model to relate the internal inductance and plasma density,

$$l_i(n_e) = \begin{cases} (l_{i,max} - l_{i,min})\frac{n_e/n_{\rm G}-0.7}{0.3} + l_{i,min} & \text{if } n_e/n_{\rm G} > 0.7 \\ l_{i,min} & \text{if } n_e/n_{\rm G} \leq 0.7 \end{cases}, \tag{13}$$

An example of the *ad hoc* relation and four alternatives relations between internal inductance and plasma density is shown in Fig. 1. Later in this work, it will be shown that the the thermo-resistive model is robust to the internal inductance model. With $q_0, q_{\rm edge}$ and n_e chosen, ν and thus the equilibrium can be solved from Eq. (10-13).

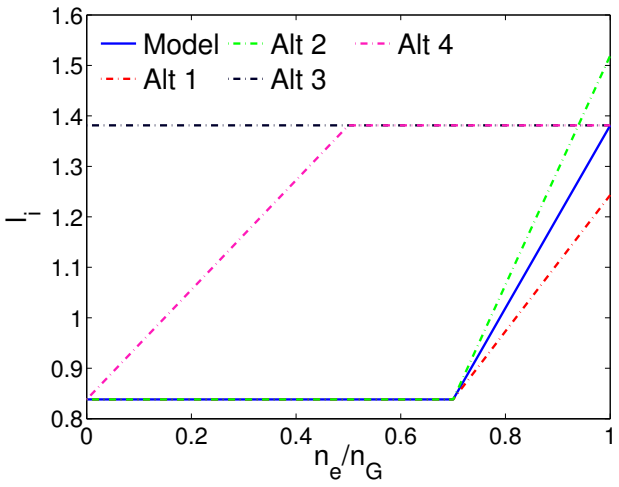

FIG. 1: The *ad hoc* and alternative models of internal inductance evolution with plasma density. The solid line is the internal inductance model given by Eq. (11)-(13). The dashed lines are four alternatives for comparison. In this case, $q_{\rm edge} = 3.7$.

Electron resistivity is calculated by $\eta = E/j$. Then the Spitzer resistivity formula is used to calculate the electron temperature [13],

$$\eta = \frac{\sqrt{2m_e}Z_{\rm eff}e^2 ln\Lambda}{12\pi^{3/2}\epsilon_0^2 T_e^{3/2}} \times \frac{1 + 1.198Z_{\rm eff} + 0.222Z_{\rm eff}^2}{1 + 2.966Z_{\rm eff} + 0.753Z_{\rm eff}^2}, \tag{14}$$

where the effective charge $Z_{\rm eff} = (n_D + \sum_Z n_Z\langle Z_Z\rangle^2)/n_e$ is a function of T_e, n_D and n_Z are deuterium and impurity densities respectively, $\langle Z_Z\rangle$ is the average charge state of impurities. Fig. 2 shows the temperature at the rational surface decreases as plasma density approaches the density limit. Auxiliary heating, which typically peaks in the center, is short-circuited along the island's separatrix and doesn't influence the local power balance inside the island.

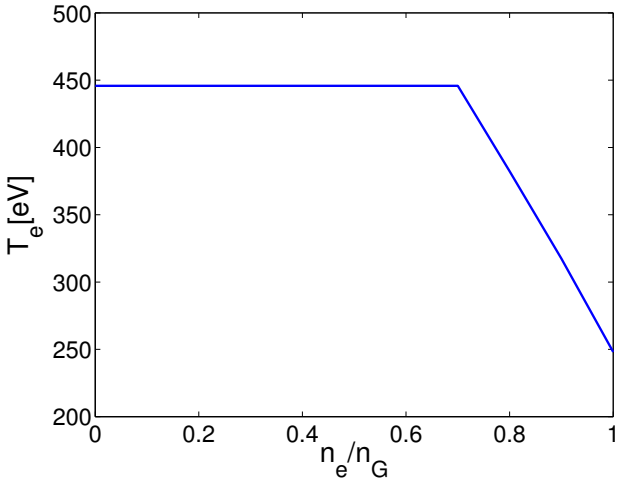

FIG. 2: An example of the temperature at the rational surface evolution with plasma density using the *ad hoc* model. The related parameters are the same as Fig. 4.

So the local power balance inside the island is dominated by Ohmic heating and radiative cooling. The local input power density is simply given by,

$$P_{\text{input}} = \eta j^2. \tag{15}$$

Plasma is cooled through Bremsstrahlung continuum radiation as well as impurity line radiation. Cyclotron radiation is ignored since a fusion plasma is normally optically thick for this range of frequencies. The power loss is calculated by [9, 14],

$$P_{\text{loss}} = n_e n_D L_D(T_e) + \sum_Z n_e n_Z L_Z(T_e), \tag{16}$$

where the cooling rate of deuterium $L_D = 5.35 \times 10^{-37} T_e^{1/2} [\text{keV}] \text{W} \cdot \text{m}^3$, and L_z is the cooling rate of impurity species Z. It's found that a small amount of high Z impurities can greatly increase radiation power while not changing Z_{eff} much. This is one of the reasons why this thermo-resistive model is so robust.

Now consider a sequence of equilibria with increasing n_e as well as fixed q_0 and q_{edge}. This sequence is shown in Fig 3, which also shows the density limit as given by Eq. (11) and the stability boundary of the tearing mode. As the density increases the current channel shrinks (decreasing r_0) and becomes more peaked (increasing ν). When the island is much smaller than w_F, the classical linear $\Delta^{'}$ determines island growth. $\Delta'_{\delta j}$ and Δ'_A dominate only when the island is sufficiently large. Thus our present cylindrical model requires a finite size seed island, i.e. the island being linearly unstable or due to perturbation from other sources.

The red line in Fig. 3 shows a characteristic equilibrium evolution path: when the plasma

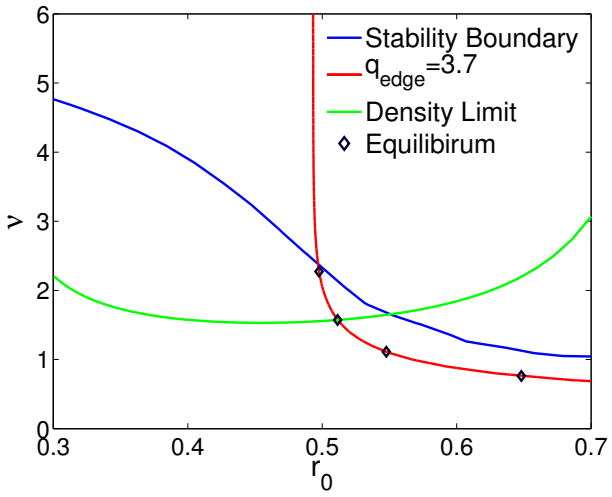

FIG. 3: A characteristic equilibrium evolution with increasing plasma density. a) The blue line: the island stability boundary in equilibrium parameter space ν, r_0, under which the island is linearly unstable. b) The red line: a characteristic equilibrium evolution path with $q_{\rm edge} = 3.7$. c) The black diamonds: equilibria with $n_e = 0.8, 0.9, 1.0, 1.1$ respectively. d) The green line: the density limit given by Eq. (11). In this case, $q_0 = 0.9$.

density is increased towards the density limit, the island approaches the stability boundary.

To calculate experimentally relevant results, parameters are chosen as: major radius $R =$ 1 meter, minor radius $a = 0.33$ meter, $q_0 = 0.9$, $q_{\rm edge}$ varied from 3.3 to 6, toroidal magnetic field B_ϕ varied from 1 to 4 T, constant toroidal electric potential U = 1 V, carbon density $n_c = 1\% n_e$, iron density $n_{Fe} = 1.1\times10^{-4} n_e$ (referred to as the normalized impurity density in this paper) and cross field electron thermal diffusivity inside the island $\chi_\perp = 0.13$ m^2/s[15]. Here iron represents the effect of all medium- to high-Z impurities; thus the density is larger than actual iron density in experiments. Impurity densities are assumed to be proportional to plasma density which may not necessarily be true. But it will be shown later in this work that the dependence of the density limit on impurities is weak. The reduction of $\chi_\perp$ is due to reduced turbulent transport inside the island.

A characteristic local power balance inside the island with increasing plasma density under the parameters above except for $q_{\rm edge} = 3.7$, $B_\phi = 3$ T is shown in Fig. 4. As n_e increases, the current channel shrinks thus j at the rational surface decreases, hence $P_{\rm input}$ drops. Meanwhile, $P_{\rm loss}$ is roughly proportional to n_e^2 and increases. So the net power is

positive before reaching the density limit thereby suppressing the island growth. And it's balanced close to the density limit. When plasma density is above the density limit the net power is negative thus enhancing the island growth.

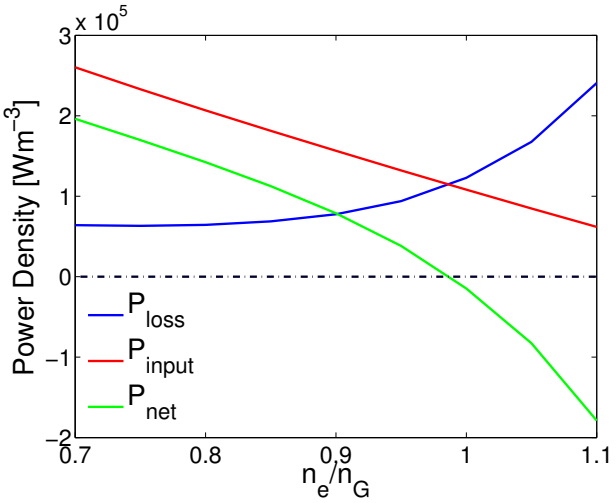

FIG. 4: An example of power balance with increasing plasma density using the *ad hoc* l_i model and the normalized impurity density. a) The blue line: the radiative cooling. b) The red line: the Ohmic heating. c) The light green line: the net input power.

In order to predict the density limit, a criterion for disruption has been chosen to be island width growing above 20% of the minor radius. Results are insensitive to the choice of the threshold island width because once island cooling occurs the island grows rapidly. A scan of the plasma density is performed using the parameters mentioned above and the result is shown in Fig. 5. Our choice of parameters covers the plasma density from 2×10^{19} m^{-3} to 2×10^{20} m^{-3}, which includes the operation regime of most tokamaks. The local power balance criterion (the blue triangles) and island width criterion (the blue squares) both agree with the Greenwald density limit within 3%. The very sharp limit is determined by the strong dependence of radiative loss on plasma density and the strong sensitivity of island growth to local power balance. This explains why the Greenwald density limit is such a robust phenomenon found across different tokamaks. Every tokamak includes impurities causing radiative cooling and leading to disruption at some plasma density. The minimum irreducible amount of impurities determines the upper limit of plasma density at which a tokamak can operate.

The impact of impurity densities on the density limit is isolated by fixing the internal

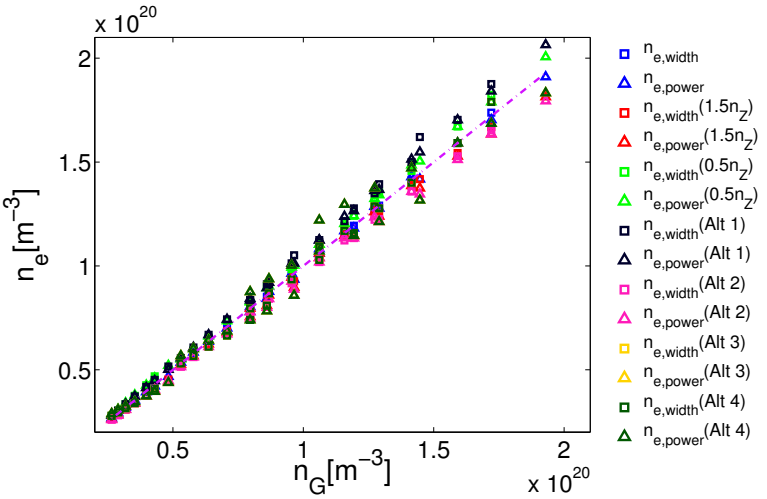

FIG. 5: Scans of the density limit. The squares are the density limit from the island width criterion. The triangles are from the local power balance criterion. a) The blue points are calculated with the normalized impurity density and the *ad hoc* l_i model given by Eq. (11)-(13). b) The red points: 1.5 times the normalized impurity density. c) The light green points: 0.5 times the normalized impurity density. d, e, f, g) The black, purple, yellow, green points: Alt 1, Alt 2, Alt 3, Alt 4 l_i models.

inductance, shown in Fig. 6. In this case, the same parameters as above are used except for $q_{\rm edge} = 4, B_\phi = 3$ T. Changing impurity densities by an order of magnitude, the density limit varies by no more than 2.5 times. This is because when impurity densities are increased, Z_{eff} increases and T_e increases as η is fixed. The cooling rate L_Z then decreases. This effect is canceling the impact of impurity densities on radiation power. It's the same when impurity densities are decreased. Thus the dependence of the power balance as well as the density limit on impurity densities is weaker than $n_Z^{0.5}$. This leads to a universal density limit scaling law spanning different tokamaks.

The stiffness of this thermo-resistive tearing mode formalism is checked by varying the parameters we use. As shown in Fig. 5, the impurity densities is varied by 50%, and four alternative internal inductance models are tested. Even in the most extreme cases, these models still predict the density limit within 15% of deviation. This justifies the assumptions of the impurity density and the *ad hoc* internal inductance model in this formalism by showing its insensitivity to these assumptions.

In this work, we reproduced the Greenwald density limit with a deviation of $\sim 3\%$ using

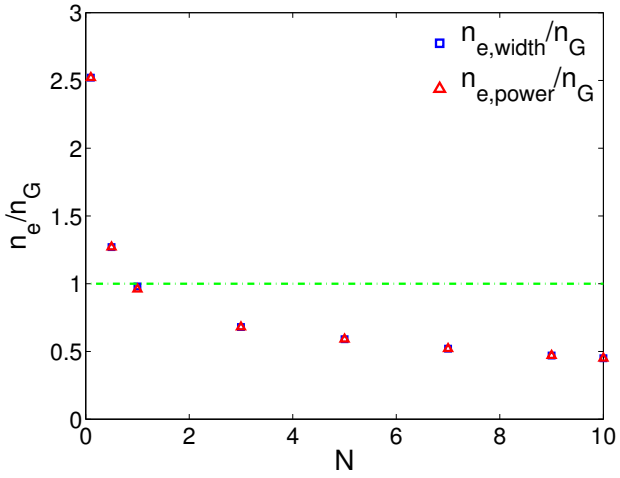

FIG. 6: Impact of impurity densities on the density limit. Here we use the Alt 3 constant internal inductance model. N represents the ratio of n_c and n_{Fe} over their values in the normalized impurities densities case.

representative experimental parameters. The thermo-resistive tearing mode model predicts the robust onset of a 2/1 tearing mode, as observed in experiments. The power balance criterion predicted by the model is a very accurate criterion for the density limit. The robustness of this model is proved by its insensitivity to the parameters we used. However, this model is still simplified and limited in many aspects. Future publications will explore the effects of toroidal geometry, nonlinear mode coupling and turbulence effects on particle, heat and impurity transport. The higher order islands may grow first from radiative cooling since they are closer to the impurity sources and are in a low temperature region of the plasma. The mechanism for rapid exponential island growth presented in this work should be robust given any island of sufficient size, thus leading to an inward propagating collapse and disruption.

[1] M. Greenwald, Plasma Physics and Controlled Fusion **44**, R27 (2002).

[2] J. Wesson, R. Gill, M. Hugon, F. Schüller, J. Snipes, D. Ward, D. Bartlett, D. Campbell, P. Duperrex, A. Edwards, *et al.*, Nuclear Fusion **29**, 641 (1989).

[3] P. Rebut and M. Hugon, Plasma Physics and Controlled Nuclear Fusion Research, London (IAEA 1985) **2**, 197 (1984).

[4] W. Suttrop, K. Buchl, J. Fuchs, M. Kaufmann, K. Lackner, M. Maraschek, V. Mertens, R. Neu, M. Schittenhelm, M. Sokoll, *et al.*, Nuclear fusion **37**, 119 (1997).

[5] D. A. Gates and L. Delgado-Aparicio, Physical review letters **108**, 165004 (2012).

[6] D. A. Gates, D. P. Brennan, L. Delgado-Aparicio, and R. B. White, Physics of Plasmas **22**, 060701 (2015).

[7] R. B. White, D. A. Gates, and D. P. Brennan, Physics of Plasmas **22**, 022514 (2015).

[8] D. P. Brennan, Q. Teng, D. A. Gates, L. Delgado-Aparicio, and R. B. White, Physics of Plasmas (2015), to be submitted.

[9] L. Delgado-Aparicio and D. A. Gates, Physics of Plasmas (2015), to be submitted.

[10] R. B. White, D. Monticello, M. N. Rosenbluth, and B. Waddell, Physics of Fluids **20**, 800 (1977).

[11] R. Fitzpatrick, Physics of Plasmas **2**, 825 (1995).

[12] P. H. Rutherford, Physics of Fluids **16**, 1903 (1973).

[13] A. Kuritsyn, M. Yamada, S. Gerhardt, H. Ji, R. Kulsrud, and Y. Ren, Physics of Plasmas **13**, 055703 (2006).

[14] D. E. Post, R. Jensen, C. Tarter, W. Grasberger, and W. Lokke, Atomic data and nuclear data tables **20**, 397 (1977).

[15] S. Inagaki, N. Tamura, K. Ida, Y. Nagayama, K. Kawahata, S. Sudo, T. Morisaki, K. Tanaka, T. Tokuzawa, *et al.*, Physical review letters **92**, 055002 (2004).

PPPL PRINCETON PLASMA PHYSICS LABORATORY

Princeton Plasma Physics Laboratory
Office of Reports and Publications

Managed by
Princeton University

under contract with the
U.S. Department of Energy
(DE-AC02-09CH11466)

P.O. Box 451, Princeton, NJ 08543
Phone: 609-243-2245
Fax: 609-243-2751

E-mail: publications@pppl.gov

Website: http://www.pppl.gov